spikes. Those wake spikes which did occur in the two-dimensional bed occurred in bubbles with diameters which were of the same order as the thickness of the bed, and they were not truly two dimensional. Of the 5,773 bubbles observed, a total of 9.8% was double bubbles, and 0.47% exhibited the jet spray mechanism.

These double-bubble frequency data agree well with the results of Rowe and Partridge (1965), who reported that 11% of the bubbles observed in their three-dimensional bed was coalescing.

ACKNOWLEDGMENTS

This research is supported by the National Science Foundation under grant CPE-7926053. The authors are also grateful to Prof. Charles Smith and the Air Force Office of Scientific Research for the use of the video system which was purchased under contract F49620-78-C-0071 and to Prof. James V. D. Eppes for his assistance with the photography.

NOTATION

d_{pi} = particle diameter
$\bar{d}_p$ = mean particle diameter
D_{FS} = bubble diameter at free surface of bed
U = superficial gas velocity
U_{mf} = superficial gas velocity at minimum fluidization
X_t = $(U/U_{mf}) - 1$
ϵ_{mf} = voidage at minimum fluidization
ρ_s = particle density

LITERATURE CITED

Chen, T., and S. Saxena, "A Theory of Solids Projection from a Fluidized Bed Surface as a First Step in the Analysis of Entrainment Processes," *Fluidization*, ed. J. Davidson and D. Keairns, Cambridge University Press (1978).

Do, H., J. Grace, and R. Clift, "Particle Ejection and Entrainment from Fluidized Beds," *Powder Technology*, **6**, 195 (1972).

George, S., and J. Grace, "Entrainment of Particles from Aggregative Fluidized Beds," *AIChE Symp. Ser.*, No. 176, **74**, 67.

Horio, M., A. Taki, Y. Hsieh, and T. Muchi, "Elutriation and Particle Transport Through the Freeboard of a Gas Solid Fluidized Bed," *Fluidization*, ed., J. Grace and J. Matsen, Plenum Press (1980).

Leva, M., and C. Wen, "Elutriation," *Fluidization*, ed., J. F. Davidson and D. Harrison, Academic Press (1971).

Rowe, P. N., and B. A. Partridge, "An X-Ray Study of Bubbles in Fluidized Beds," *Transactions Institution of Chemical Engineers*, **43**, T157 (1965).

Rowe, P. N., B. A. Partridge, A. G. Cheney, G. A. Henwood, and E. Lyall, "The Mechanisms of Solids Mixing in Fluidized Beds," *Trans. Instn. Chem. Engrs.*, **43**, T271 (1965).

Zenz, F. A., and N. A. Weil, "A Theoretical-Empirical Approach to the Mechanism of Particle Entrainment from Fluidized Beds," *AIChE J.*, **4**, 472 (1958).

Manuscript received July 7, 1981, revision received March 2, and accepted April 30, 1982.

Distributed Pore-Size Model for Sulfation of Limestone

A model is proposed to study the reaction between a porous solid and a reactant gas resulting in solid and gaseous products. The model describes the reacting solid as a sphere made up of a distribution of randomly oriented open pores. The evolution of the pore-size distribution is followed by use of a population balance, using a combination of the independent variables of time and location first presented by Dudukovic (1976). The macroscopic properties of the solid are obtained by integrating over the pore size distribution. The results of the population balance are used with a mass balance on the reacting gas to obtain rate and conversion data.

The results of the model are compared to experimental data obtained for the sulfation of limestone (Ulerich et al., 1977). Both rate vs. conversion as well as conversion vs. time plots are presented, which serve as a more strenuous test of the model than either type of plot alone.

P. G. CHRISTMAN
Department of Chemical and Nuclear Engineering
University of California
Santa Barbara, CA 93106

T. F. EDGAR
Department of Chemical Engineering
The University of Texas at Austin
Austin, TX 78712

SCOPE

The distributed pore model is the first attempt to characterize the solid structure, in a gas/solid reaction undergoing pore closure, with a distribution of pore sizes instead of an average grain or pore size. This model accounts for four resistances to the overall reaction. These resistances include mass transfer across a mass transfer boundary layer, through the porous medium and through the solid product as well as surface reaction kinetics. The relative importance of the resistances depends on both the initial pore size and the extent of conversion. One feature of most previous models based on an average pore or grain size was a sudden cut off of the reaction at the point of pore closure. The experimental data do not show this type of behavior but the rate tends to gradually decrease as the outer layer is plugged. Hartman and Coughlin (1976) overcame this problem with their grain model by noting that a certain amount

of residual porosity associated with the largest pores remained after the bulk of the outer shell was plugged. By using this residual porosity as an adjustable parameter they obtained a smooth decrease in the reaction rate up to the ultimate conversion.

In this paper the results of the distributed pore-size model are compared to the data of Ulerich et al. (1977) for the sulfation of calcined limestone. The model predicts a gradual decrease in the rate as reaction proceeds, as observed from the data. This gradual decrease comes directly from the assumptions of the model which follows the behavior of pores of all sizes without resorting to an artificial residual porosity.

CONCLUSIONS AND SIGNIFICANCE

By considering the solid as a porous medium with a distribution of sizes, the distributed pore model is able to eliminate one of the weaknesses of previous pore closure models. The existence of a small porosity associated with only the largest pores, observed by Hartman and Coughlin (1976), is predicted as a natural consequence of the models initial assumptions.

The major limitation of the model is associated with its neglect of the existence of pore intersections as reaction proceeds. This does not seem to be a serious factor for conversions of less than 50% as observed in the limestone-SO_2 system studied in this paper, but it would become much more important for systems where the ultimate conversion approached 100%. The model would tend to overpredict the local reaction rate near complete conversion.

The model predictions are in excellent agreement with experimental data of Ulerich et al. (1977) for local conversions less than 50%. The significance of the pore size distribution is illustrated by a comparison of three experiments performed on calcined limestone with different pore size distributions. The model shows that the differences in the kinetic behavior of these calcined limestones can be attributed to the different pore structures. It further shows these pore structures affect macroscopic behavior of the reacting pellets.

INTRODUCTION

Early mathematical models to stimulate gas/solid, noncatalytic reactions involving solid products have included the sharp interface shrinking core models discussed in detail by Szekely et al. (1976). More advanced are the grain models presented by Szekely and Evans (1970, 1971), Wen and Ishida (1973) and Calvelo and Smith (1971), and the pore models of Szekely and Evans (1970) and Chu (1972). These were the first models to incorporate structural properties of the solid as parameters of the model instead of incorporating them into an empirical reaction rate constant. These models, however, do not incorporate changes in the structural properties with extent of reaction. Hartman and Coughlin (1976) noted that the porosity of limestone decreased with extent of reaction and incorporated this effect into a modified grain model. Georgakis, Chang, and Szekely (1979) extended this idea with their changing grain size model by noting that the loss of porosity must be due to increases in grain size with extent of reaction. Ramachandran and Smith (1977a) and Chrostowski and Georgakis (1978) improved upon the single pore models by taking into account changes in the pore diameter with extent of reaction. Ramachandran and Smith (1977b) and Ranade and Harrison (1979) extended the grain model further to include the effects of sintering as reaction proceeds. Bhatia and Perlmutter (1980, 1981a, 1981b) have developed a random pore model which accounts for intersections among pores as well as changes in pore structure.

All of the models mentioned above suffer from the drawback that they treat the solid structure as having an average grain or pore size. This is a limiting assumption in the models where the solid structure changes with extent of reaction. In general the evolution of an average pore or grain is not representative of the evolution of a distribution of pore or grain sizes. Reaction models that follow the evolution of a complete distribution of pore sizes with extent of reaction have been presented by Schechter and Gidley (1969), Hashimoto and Silveston (1973a, 1973b) and more recently by Simons and Finson (1979) and Simons (1979). These models are concerned with reactions such as coal gasification and limestone acidification where no solid product is deposited as the result of the reaction. Simons and Finson (1979) approximated the pore size distribution with a unimodal distribution to study gasification and Simons and Rawlins (1980) applied a similar technique to study initial rate data for the reactions of CaO(s) with H_2S(g) and SO_2(g). They did not, however, consider the effect of the solid product buildup on the surface of the pores.

MODEL DESCRIPTION

Consider the general irreversible reaction

$$\beta_1 A(s) + \beta_2 C(g) \rightarrow \beta_3 B(s) + \beta_4 D(g)$$

and make the following assumptions.

(1) The reacting solid A is a porous spherical pellet which maintains its structural integrity throughout the reaction; i.e., the outer radius of the pellet remains a constant.

(2) The porous medium is made up of a distribution of open, interconnecting, cylindrical pores with a random distribution of orientations and locations.

(3) The rate of reaction is slow enough that we may neglect any thermal gradients throughout the pellet.

(4) The gas concentration depends only on time and radial position in the pellet.

(5) The net mass flux can be neglected, since the gas concentration is very small, or gases C and D are undergoing equimolar counter diffusion.

(6) Changes in the solid structure occur slowly enough so that the pseudo steady state assumption for the gas concentration profile in the pellet is valid.

The model considers four resistances to the overall chemical reaction rate:

(1) Diffusion through a boundary layer surrounding the pellet.

(2) Diffusion through the porous medium into the reacting spherical pellet.

(3) Diffusion through the solid product layer deposited on the walls of the reacting pores.

(4) First order surface reaction kinetics at the solid reactant/product interface where the reacting gas contacts the solid reactant.

The following discussion presents a mathematical deviation of the gas/solid noncatalytic reaction model considering the assumptions and resistances discussed above. Initially, we will be concerned with the structural changes that occur in a single cylindrical pore as

reaction proceeds. Then by use of a population balance on the entire pore-size distribution, the evolution of this distribution with respect to time and location in the pellet will be presented. Finally, by integrating over the pore-size distribution, the macroscopic properties necessary to obtain the pseudo steady state concentration profile in the pellet will be obtained, as well as other properties of interest.

Chemical Reaction in a Single Pore

Consider a single pore with initial radius r_o. As reaction occurs, a product layer will form on the walls of the cylinder, creating new radii r_1, at the solid-gas interface, and r_2, at the solid-solid interface between reactant A and product B, as shown in Figure 1. Finally, assume that the total gas concentration c and pore radii do not vary significantly over the distance l.

Performing a mass balance in cylindrical coordinates for the gaseous reactant with concentration c, in the product layer, diffusing through the product layer in the radial direction, the following differential equation is obtained.

$$\frac{\partial \hat{c}}{\partial t} = \frac{1}{r}\frac{\partial}{\partial r}\left[D_s r \frac{\partial \hat{c}}{\partial r}\right] \tag{1}$$

Assuming the pseudo steady state assumption holds, and applying the following boundary conditions.

$$\text{i) } \hat{c}|_{r=r_1} = c$$

$$\text{ii) } k\hat{c}|_{r=r_2} = -D_s \frac{\partial \hat{c}}{\partial r}|_{r=r_2}$$

Eq. 1 can be solved to obtain the gas concentration at the reacting surface (r_2).

$$\hat{c}(r_2) = \frac{c}{1 + r_2(k/D_s)\, ln(r_2/r_1)} \tag{2}$$

As reaction occurs the location of r_1 and r_2 will change. From the dependence of $\hat{c}(r_2)$ on r_1 and r_2, we can see that it also will change as a function of time. To determine the functionality of $\hat{c}(r_2)$ with respect to time, it is first necessary to express r_1 and r_2 as functions of time.

The rate of change of the outer radius r_2 is merely the product of the chemical reaction rate ($k\hat{c}(r_2)$), the molar volume V_A of reactant A and the ratio of the stoichiometric coefficients (β_1/β_2).

Combining this relationship with Eq. 2, an expression for the rate of change of r_2 as a function of the gas reactant concentration is obtained.

$$\left[\frac{\partial r_2}{\partial t}\right]_{r_o} = \frac{(\beta_1/\beta_2)V_A kc}{1 - r_1(k/D_s)\, ln(r_2/r_1)} \tag{3}$$

From the reaction stoichiometry and definitions of r_1 and r_2 it can be shown that the three characteristic radii of the pore are related by Eq. 4.

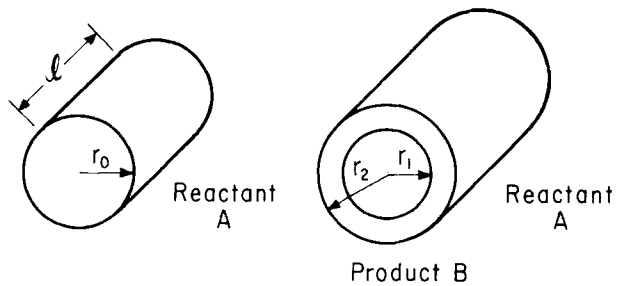

Figure 1. Geometric changes in a short cylindrical pore due to chemical reaction forming a product with a different molar volume than that of the product.

$$r_1^2 = \alpha r_o^2 + (1 - \alpha) r_2^2 \tag{4}$$

where:

$$\alpha = \frac{\beta_3 V_B}{\beta_1 V_A}$$

Alpha is the effective ratio of the molar volumes of the solid product and reactant.

Taking the derivative of Eq. 4 and combining the resulting equation with Eq. 3 yields an expression for the rate of change of r_1 with respect to time holding r_o constant.

$$\left[\frac{\partial r_1}{\partial t}\right]_{r_o} = \frac{(\beta_1/\beta_2)V_A k(1 - \alpha)(r_2/r_1)c}{1 + r_2(k/D_s)\, ln(r_2/r_1)} \tag{5}$$

Equation 5 shows that the rate of change of r_1 depends on both of the characteristic radii, r_1 and r_2, and the concentration of the gas reactant. But the gas reactant concentration is a function of both time and the pore location in the pellet. Thus, Eq. 5 is coupled to an overall mass balance of the pellet which is required to obtain $c(R,t)$, where R represents the location of the pore in the pellet. Furthermore, the mass balance over the pellet depends on the characteristics of all pores, of all sizes at every location in the pellet.

Equation 5 can be decoupled from the rest of the system by defining a new parameter τ such that

$$\tau \equiv \int_o^t \frac{c(R,t)}{c_o} dt \tag{6}$$

where c_o is the gas concentration at the surface of the pellet ($R = R_o$). Thus, τ has the same value as time for the reaction under kinetic control. This is the same transformation first done by Dudukovic (1976) and he calls τ the cumulative gas concentration. Differentiating Eq. 6 with respect to time and applying the chain rule to Eq. 5 we obtain an expression for the rate of change of r_1 with respect to τ.

$$\left[\frac{\partial r_1}{\partial \tau}\right]_{r_o} = \frac{(\beta_1/\beta_2)V_A k(1 - \alpha)(r_2/r_1)c_o}{1 + r_2(k/D_s)\, ln(r_2/r_1)} \tag{7}$$

In Eq. 7 time and location are combined into one variable τ. In contrast, in Eqs. 3 and 5 the characteristic radii depend on time explicitly and on time and location implicitly because of the dependence of $c(R,t)$. Equation 7 may now be integrated as a function of τ without considering the functionality of $c(R,t)$.

Since both r_1 and r_2 depend on τ, Eq. 7 can be combined with Eq. 4 to yield an expression for $[\partial r_1/\partial \tau]_{r_o}$ that depends on τ and r_1 only. Integrating this equation while holding r_o constant and noting that $r_1 = r_o$ when $\tau = 0$ yields τ explicitly as a function of r_1 and r_o.

$$\tau = \frac{(1 - \alpha)r_o}{\lambda k}\left\{1 - \left[\frac{\alpha - (r_1/r_o)^2}{\alpha - 1}\right]\right\} + \left(\frac{r_o^2}{4\lambda D_s}\right)\left\{\left(\frac{r_1}{r_o}\right)^2 ln(r_1/r_o)^2 - \left(\left(\frac{r_1}{r_o}\right)^2 - \alpha\right) ln\left[\frac{(r_1/r_o)^2 - \alpha}{1 - \alpha}\right]\right. \tag{8}$$

where

$$\lambda \equiv (\beta_1/\beta_2)V_A c_o(\alpha - 1) \tag{9}$$

Equation 8 is an analytical expression which relates to r_1 and r_o. Thus if the gas concentration history in the vicinity of a pore of initial radius r_o is known, the inner radius r_1 can be obtained from Eq. 8 and the outer radius r_2 can be obtained by using Eq. 4. This significantly reduces the numerical effort required to solve the model.

The use of r_1 as the dependent variable is advantageous for all cases where $\alpha > 1$ because it becomes zero when the pore is plugged and therefore nonreactive. However, this choice causes some problems when $\alpha = 1$. For that case r_1 will not change with the extent of reaction and Eq. 9 yields indeterminate results. We feel, however, that the benefit of using r_1 as the dependent variable outweighs the disadvantage associated with the unique case where r_1 is not a function of conversion.

Evolution of Pore-Size Distribution

In the spherical pellet, there exists a distribution of pores which intersect the surface of the shell located at R. The distribution is defined by a distribution function $\eta_1(r_1,R,t)dr_1$, which is the number of pores with sizes between r_1 and $r_1 + dr_1$ intersecting a unit surface at R. It is assumed that the pores are randomly oriented in the porous matrix independent of size r_1 and that the average length (l) of the pores is small with respect to the radius of the pellet.

Performing a population balance over the pore size distribution generates the following partial differential equation.

$$\frac{\partial \eta_1(r_1,R,t)}{\partial t} + \frac{\partial}{\partial r_1}\left[\eta_1(r_1,R,t)\frac{\partial r_1}{\partial t}\right] = \eta_1(r_1,R,t)\frac{\partial \phi(r_1,R,t)}{\partial t} \tag{10}$$

where $(\partial\phi/\partial t)$ represents the net rate of the net fractional increase in the number of pores due to pore intersections.

By employing the chain rule, we can transform Eq. 10 from an equation in time to an equation in the variable τ.

$$\frac{\partial \eta_1(r_1,\tau)}{\partial \tau} + \frac{\partial}{\partial r_1}[\eta_1(r_1,\tau)\xi_1(r_1,\tau)] = \eta_1(r_1,\tau)\frac{\partial \phi(r_1,R,\tau)}{\partial \tau} \tag{11}$$

where

$$\xi_1 \equiv (\partial r_1/\partial \tau) \tag{12}$$

The use of the variable τ generates the decoupled Eq. 11 from Eq. 10 just as Eq. 7 was generated from Eq. 5.

Only in a few cases can analytical solutions to this type of equation be obtained. Previous authors have succeeded in solving for the moments of the distribution η_1 as a function of time, and using these moments to calculate the required macroscopic properties. This requires a fairly simple form for the reaction term ξ_1. As can be seen from Eq. 7 this term is not a simple function for the case under consideration. Therefore, a numerical solution is required.

There are no mechanisms by which two pores may interact to produce a new single pore in a reaction system where a solid product is formed. However, pores may be destroyed or partially destroyed via two possible mechanisms. When the inner radius of a pore (r_1) reaches zero, a pore no longer exists. When two pores are close enough that their outer radii (r_2) at the reaction front overlap, part of the surface available for reaction to both pores is eliminated. The former mechanism can be handled easily whereas the second mechanism requires a more extensive analysis. In this paper we will only consider the loss of pores due to plugging, and will not include the effect of intersections.

A plugged pore contributes nothing to the diffusivity, reactivity, porosity, or any other macroscopic property of the porous medium. It makes no difference if these pores are counted or not. If all pores with radii of zero that initially had some finite radius r_o are counted, then the total number of pores in this reaction process is conserved and $\partial\phi/\partial t = 0$. Thus we can say in the absence of pore intersections.

$$\frac{\partial \eta_1}{\partial \tau} + \frac{\partial}{\partial r_1}\left(\eta_1 \frac{\partial r_1}{\partial \tau}\right) = 0 \tag{13}$$

This greatly simplifies solution of the population balance. The required initial and boundary conditions can be obtained from the initial pore size distribution.

Chemical Reaction in Porous Medium

By integrating over the properties of the individual pores multiplied by the pore size distribution function $\eta_1(r_1,\tau)$ the macroscopic properties of the porous matrix can be determined. Thus the void area per unit area ψ is

$$\psi = \int_o^\infty \pi r_1^2 \eta_1 dr_1 \tag{14}$$

Petersen (1957) and Schechter and Gidley (1969) have shown that for randomly oriented pores the void area per unit area is equal to the void volume per unit volume, and thus the porosity ϵ is

$$\epsilon = \int_o^\infty \pi r_1^2 \eta_1 dr_1 \tag{15}$$

This relationship is very important, and can be used in conjunction with mercury porosimetry to experimentally determine the initial form of η_1. All other macroscopic properties that are required may be determined in a similar manner by integrating over the properties of the individual pores.

Performing a mass balance on reactant gas C undergoing diffusion and chemical reaction in a spherical porous pellet yields

$$\frac{1}{R^2}\frac{\partial}{\partial R}\left[R^2 D_e \frac{\partial c}{\partial R}\right] = K_e c \tag{16}$$

where

$$D_e = \frac{1}{\zeta}\int_o^\infty (\pi r_1^2) D_c \eta_1 dr_1 \tag{17}$$

$$K_e = 2k\int_o^\infty \frac{\pi r_2 \eta_1}{1 + r_2(k/D_s)\,ln(r_2/r_1)}dr_1 \tag{18}$$

$$D_c = \left(\frac{1}{D_B} + \frac{1}{D_K(r_1)}\right)^{-1} \tag{19}$$

A detailed derivation of this mass balance is presented by Christman (1981). Equation 17 is of the same form derived by Johnson and Stewart (1965) for diffusion in catalyst pellets.

For systems involving diffusion and chemical reaction in a porous catalyst pellet it is assumed that the diffusivity is not a function of R, and it is combined with the reaction term to define a Thiele modulus. This generates a differential equation that can be solved analytically for the concentration profile. In Eq. 16, however, D_e is a function of both time and location because it depends on the pore-size distribution $\eta_1(R,t)$. Similarly, K_e depends on time and location through its dependence on $\eta_1(r,t)$. Thus, Eq. 16 must be solved numerically for each time to determine the pseudo steady-state concentration profile. By applying the following boundary conditions, Eq. 16 can be solved to obtain the gas concentration profile in the pellet.

$$i)\ R = 0 \quad \frac{dc}{dR} = 0 \tag{20}$$

$$ii)\ R = R_o \quad \left(D_e \frac{dc}{dR}\right) = k_g(c_o - c) \tag{21}$$

where k_g = mass transfer coefficient.

The first boundary condition exploits the symmetry of the model system. The second merely states that the rate of diffusion to the outer surface of the pellet is equal to the rate of diffusion into the pellet.

The properties determined so far are sufficient to build a self-consistent numerical model of the reaction system of interest. There are, however, two other macroscopic properties that are of interest, the fractional conversion of reactant A to product B and the rate of reaction or rate of change of conversion.

It can be shown that the conversion can be expressed as a function of the porosity, the initial porosity and alpha ($\alpha \neq 1$) as

$$x(R,t) = \frac{\epsilon_o - \epsilon(R,t)}{(1 - \epsilon_o)(\alpha - 1)} \tag{22}$$

Since $\epsilon(R,t)$ can be determined directly from Eq. 15, Eq. 22 serves as a convenient way to determine the conversion without integrating over the pore-size distribution.

The rate of change of conversion with time can be obtained directly from the equivalent reactivity K_e. From the definition of K_e in Eq. 31, it can be shown that the rate of consumption of gas C per unit volume of the porous medium is the equivalent reactivity times the gas concentration ($K_e c$). From the stoichiometry of the reaction and the definition of conversion the rate of change of conversion for pure reactant A can be shown to be

$$\frac{dx}{dt} = \left(\frac{\beta_1}{\beta_2}\right)\left(\frac{V_A K_e c}{1-\epsilon_o}\right) \tag{23}$$

The fact that the conversion and the rate of change of conversion can be calculated independently of each other provides a check on the numerical methods used.

In addition to determining values of local properties (at each grid point), the values of overall properties, which are more easily measured, are also determined. These values, such as the overall porosity, conversion, and overall reaction rate, are determined by a volume-weighted integration over the local property of interest.

NUMERICAL SOLUTION TECHNIQUE

The model, as described above can be solved numerically. This requires four basic steps.

1. Solution of the evolution equation to determine how the pore size distribution varies as a function of τ.
2. Determination of the macroscopic properties (D_e, K_e, ϵ) as a function of τ.
3. Solution of the mass balance to determine the pseudo-steady-state concentration profile of the reacting gas.
4. Integration of the local macroscopic properties over the entire pellet to obtain the observed conversion and reaction rate for the pellet.

The first step is accomplished by choosing specific values of r_o and r_1 and generating values of τ from Eq. 8. This information may then be used in tabular form to determine r_1 as a function of r_o and τ. A cubic spline is used to interpolate values of r_1 between values that are tabulated. This allows Eq. 13 to be solved to determine $\eta_1(r_1,\tau)$, using the initial distribution $\eta_o(r_o,0)$ determined from the measured pore-size distribution.

The macroscopic properties (D_e, K_e, ϵ) are determined by integrating Eqs. 17, 18 and 15, respectively, at various values of τ where $\eta(r_1,\tau)$ is known. All of these integrations are carried out using Gauss-Lengendre quadrature. These values are then tabulated as a function of τ. A cubic spline is then fit through the tabulated values for purposes of interpolation.

Equation 16 is solved to determine the pseudosteady-state gas concentration profile. This is done using a 50 point centered space finite differencing scheme and solving the resultant tridiagonal matrix. Initially it is assumed that the gas concentration $c(R)$ is constant at each grid point over the small time step (Δt). Then $\Delta\tau$ is determined at each point from Eq. 6. Next the macroscopic properties are determined from their dependence on τ. Then Eq. 16 is solved again to determine the gas concentration at the end of the time step using the updated macroscopic properties. An updated value of $\Delta\tau$ is then determined by applying the trapezoidal rule to Eq. 6. This procedure is continued until there is no significant change in the local reaction rate $(K_e c)$ at any grid point. This variable was chosen because it is sensitive to changes in both the concentration profile and the extent of conversion in the porous matrix.

After each time step is completed, the overall conversion and overall change in conversion with time is determined by repeated use of Simpson's Integration formula. Then a new time step is initiated using the updated values of τ and the macroscopic properties. This implicit method is continued until the desired reaction time is reached.

RESULTS

Ulerich et al. (1977) have obtained data for the sulfation of calcined limestone in a thermogravimetric analyzer (TGA). The calcination was performed prior to the sulfation in a laboratory-scale fluidized bed. The sulfation reaction is shown below:

$$CaO(s) + SO_2(g) + \tfrac{1}{2}O_2(g) \rightarrow CaSO_4(s)$$

The sulfation experiments were carried out at 815°C on pre-calcinated samples with known pore-size distributions. The sulfur dioxide concentration was maintained at a low level and the oxygen was kept in large excess. Under these conditions the sulfation can be easily described as a special case of the distributed pore-size model, where there is no product gas.

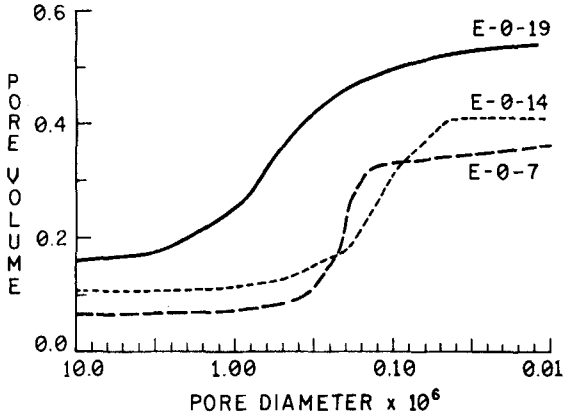

Figure 2. Pore-size distributions for calcined linestones. E-0-7, Lowellville, calcined at 815°C in 15% CO_2 for 4 hours; E-0-14, Greer, calcined at 815°C in N_2 for 4 hours; E-0-19, Lowellville, calcined at 900°C for 90 minutes in 60% CO_2 and for 150 minutes in N_2; Pore volume (m^3/kg) vs. pore diameter (m).

Experiments E-0-7, E-0-14 and E-0-19 were chosen for comparison with the predictions of the distributed pore-size model. The pore-size distributions of the calcined limestones measured by Ulerich et al. (1977) during these three experiments are presented in Figure 2. These distributions vary significantly over the three experiments. A comparison of E-0-7 and E-0-19 shows that the same limestone can produce a different pore size distribution, depending on the calcination conditions. From mineral analysis it was determined that Lowellville is very high in calcium whereas Greer has a significant amount of silica as an impurity.

Model Parameters

In Table 1 the parameters which did not vary among the three experiments are presented. These include average radius of the pellet and the $SO_2(g)$ concentration specified for the experiment. The molar volume of solids CaO(s) and $CaSO_4(s)$ were obtained from x-ray crystallographic data (Weast, 1971). The bulk diffusivity was estimated from an optimized Gilliland-type equation attributed to Fuller et al. (1966).

The surface reaction rate constant was estimated from the initial rate data plotted in the form of rate vs. conversion. The value of 1.9×10^{-3} m/s for the rate constant is in reasonable agreement with the value of 2.3×10^{-3} m/s estimated by Bhatia and Perlmutter (1981b). It however should be realized that there is significant variation in the values reported in the literature for this constant ranging from 6.6×10^{-2} m/s reported by Hartman and Coughlin (1976) to 4.2×10^{-4} m/s reported by Wen and Ishida (1973).

The diffusivity through the product layer cannot be easily measured but must be estimated from kinetic data. Thus the value obtained depends on the choice of the model used to analyze the data and thus estimates vary widely. Reported values at 850°C

TABLE 1. FIXED SIMULATION PARAMETERS

Parameter	Value
Pellet Radius (m)	6.0×10^{-4}
SO_2 Concentration (kmol/m^3)	5.6×10^{-5}
Rate Constant (m/s)	1.9×10^{-3}
Molar Volume (m^3/kmol)	
CaO	1.68×10^{-2}
$CaSO_4$	5.22×10^{-2}
Bulk Diffusivity (m^2/s)	1.25×10^{-4}
Product Layer Diffusivity (m^2/s)	4.0×10^{-12}

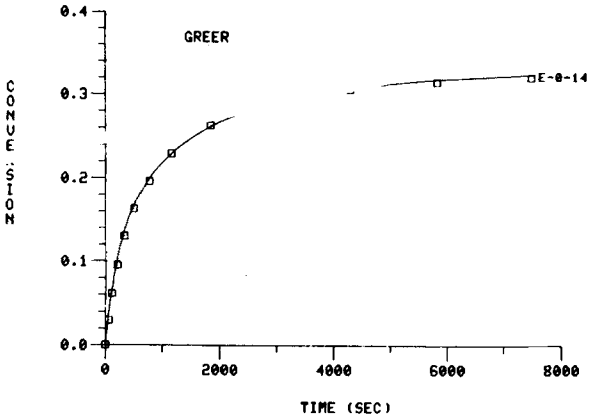

Figure 3a. Comparison of distsributed pore model with experimental data (Greer Limestone). Sulfation conditions: 815°C, 4% O_2, and 0.5% SO_2.

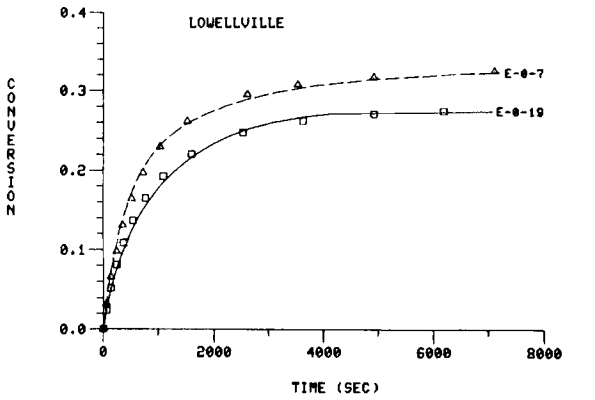

Figure 4a. Comparison of distributed pore model with experimental data (Lowellville Limestone). Sulfation conditions: 815°C, 4% O_2, and 0.5% SO_2.

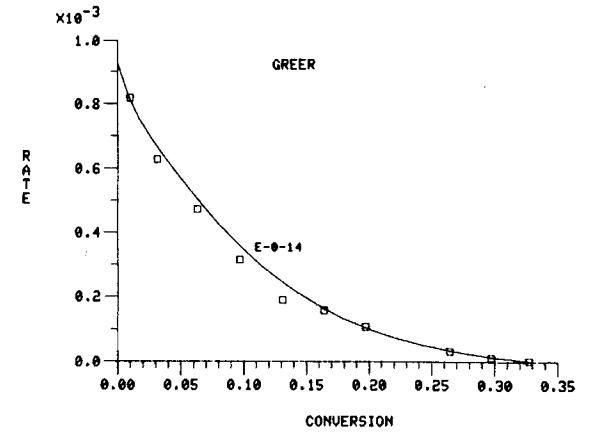

Figure 3b. Comparison of distributed pore model with experimental data (Greer Limestone). Sulfation conditions: 815°C, 4% O_2, and 0.5% SO_2.

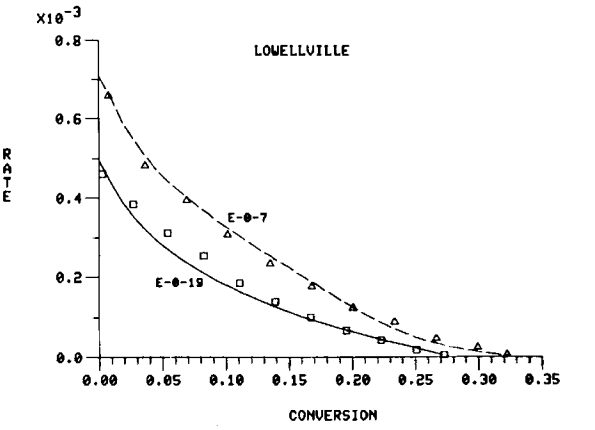

Figure 4b. Comparison of distributed pore model with experimental data (Lowellville Limestone). Sulfation conditions: 815°C, 4% O_2, and 0.5% SO_2.

TABLE 2. VARIABLE REACTION CONDITIONS AND SIMULATION PARAMETERS

Calcination Conditions	E-0-7	E-0-19*	E-0-14
Limestone	Lowellville	Lowellville	Greer
Calcination Temp. (°C)	815	900	815
CO_2 Partial Press. (kPa)**	15	60/0.0	0.0
Calcination Time (min)	240	90/150	240
Wt. Loss after Calcination (%)	40.95		39.04
Simulation Parameter			
Initial Porosity	0.50	0.43	0.48
Tortuosity (τ)	1.8	2.7	1.6
Sherwood Number	0.43	0.34	0.60

* E-0-19 was calcined for 90 min under 60 kPa CO_2 and an additional 150 min under 0.0 atm CO_2.

** The balance was N_2(g); total pressure, 101 kPa.

include 6.0×10^{-13} m^2/s (Hartman and Coughlin, 1976); 7.6×10^{-13} to 2.5×10^{-11} m^2/s (Bhatia and Perlmutter, 1981b); 8.0×10^{-13} to 2.5×10^{-10} m^2/s (Georgakis et al., 1979); and 7.5×10^{-11} to 3.0×10^{-10} m^2/s (Chrostowski and Georgakis, 1979). The value of 4.0×10^{-12} m^2/s reported in Table 1 is within this large range of reported values.

There are three parameters that, as expected, varied among the three experiments. These are the tortuosity, the Sherwood Number and the initial porosity. The values of these parameters, and the different calcination conditions of the three experiments are presented in Table 2.

When the initial pore size distributions were obtained by mercury porosimetry, the mercury penetrated interstitial volume between pellets as well as pore volume. To exclude the interstitial volume from consideration the pore size distributions shown in Figure 2 must be modified. This was done by picking a maximum pore size that can be considered. All pore volume larger than the cut-off point is considered interstitial volume. The cut-off point used for the three experiments varied from 8.8×10^{-7} m (E-0-7, E-0-14) to 6.4×10^{-7} m (E-0-19). Assuming all the pore volume smaller than the cut-off point is due to actual pores, the initial porosities of the sample were calculated and reported in Table 2.

The initial porosities reported in Table 2 are very reasonable. If the starting material were pure nonporous $CaCO_3$(s), complete calcination with no shrinkage of the original pellet would yield an expected porosity of 0.54. These samples were not pure and some shrinkage may be expected due to sintering. In fact, the sample calcined at the higher temperature (E-0-19) displays the lowest porosity, most likely due to a higher sintering rate at the higher temperature.

The values reported in Table 2 for the Sherwood Number and the tortuosity were adjusted to obtain the best fit with the experimental data. The tortuosities are in the acceptable range for natural pore systems which generally are around 2.0. The Sherwood Number ($Sh = 2k_gR_o/D_B$) varied slightly between the Lowellville runs and the Greer run. This parameter would be a function of the sample holder geometry, superficial gas velocity, particle geometry, etc. The reported values are all less than 2 (expected for a particle in a stagnant gas) because many particles were packed to perform these experiments and they interfere with each other.

Model Predictions

In Figures 3 and 4, the predictions of the model are compared to experimental data taken by Ulerich et al. (1977). In these figures, conversion is plotted vs. time and the rate of reaction is plotted vs. conversion. Conversion vs. time plots are sensitive to differences

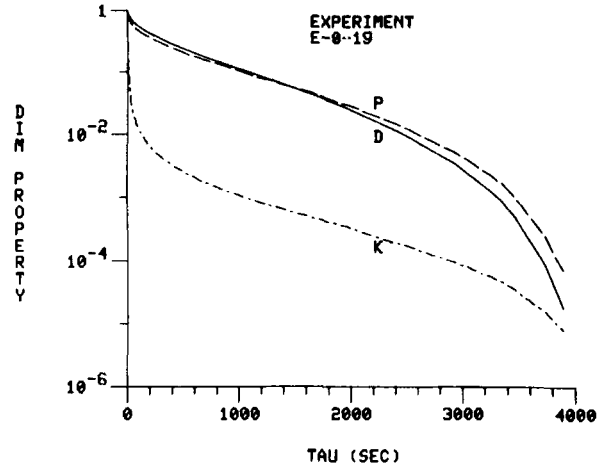

Figure 5. Change in dimensionless macroscopic properties with respect to reaction parameter, τ.

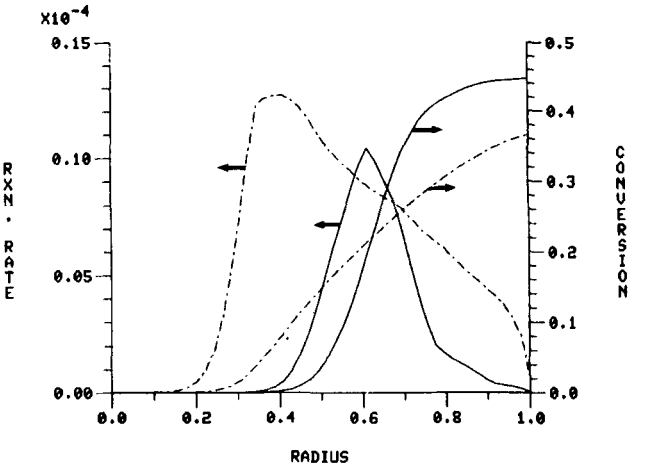

Figure 6. Local reaction rate and conversion vs. dimensionless radius just before pore plugging.

(- · -) E-0-19
(—) E-0-14

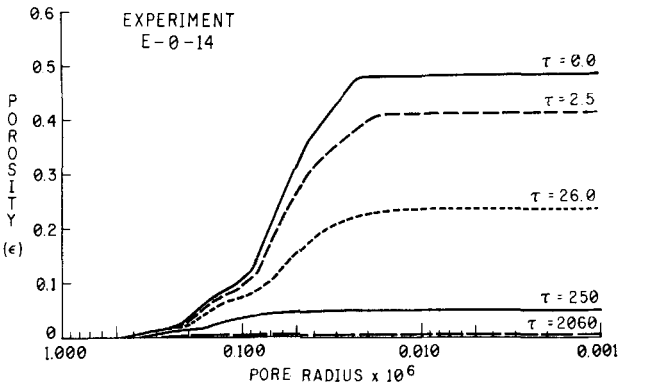

Figure 7. Evolution of pore-size distribution as a function of cumulative gas concentration τ (s). Pore volume (m^3/kg) vs. pore radius (m).

in the reaction rate at intermediate and long times. These plots however are not sensitive to predictions of the initial reaction rate. Rate vs. conversion plots are not sensitive to errors at long times but serve as good tests of the model's predictions of initial and intermediate rates of reaction. The ability of a single simulation to predict both of these curves is a good test which has not been applied to other models.

There are two features of these figures that warrant attention. The model and the data are in good agreement over a very long reaction time (2.5 h), and the rate gradually falls off before all of the pores are plugged. The reaction time is much longer than that used by Borgwardt (1970) and Hartman and Coughlin (1976) who present data obtained over periods of 120 seconds and 60 minutes respectively. Other authors (e.g., Bhatia and Perlmutter, 1981b; Chrostowski and Georgakis, 1978) have chosen to compare their model predictions to only the first 30 minutes of Hartman and Coughlin's data, even though reaction also occurs in the last 30 minutes.

Many of the previous models predict a sudden stop in the reaction rate at the time of pore plugging. Hartman and Coughlin (1976) eliminated this feature from their grain model by noting that even after one hour there were large pores on the surface of the reacted pellet. They accounted for this phenomenon by adding an adjustable parameter, the residual porosity, to their model. In contrast, a gradual decrease in the reaction rate as different-sized pores are plugged is inherent in the distributed pore size model and does not require an additional parameter.

Because of the excellent agreement between the experimental data and the model, we can treat the mechanistic predictions of the model with some confidence. In Figure 5 the ratio of the macroscopic properties of the porous media to their initial values are plotted as a function of the reaction parameter, τ, for experiment E-0-19. The dimensionless diffusivity (D), porosity (P), and the reactivity (K) are plotted logarithmically. All three of the properties decrease dramatically as the reaction proceeds. The reactivity initially decreases most dramatically as the product layer builds up. Near the pore plugging point all the properties drop off very quickly toward zero. Completely different curves were obtained for the other two experiments because of the significant differences in the pore size distributions.

The dimensionless diffusivity and porosity curves exhibit a rather interesting behavior. In all cases they exhibit three points of intersection. Initially they have a value of 1.0. As the reaction proceeds the major loss in porosity is due to reaction in smaller pores which are in the Knudsen diffusion regime. Since the Knudsen diffusion rate is less than the bulk diffusion rate in the larger pores, the fractional loss in the diffusivity is less than the fractional loss of porosity. At longer reaction times the larger pores shrink to the point where the bulk diffusion regime gives way to the Knudsen regime. When this phenomenon dominates, the diffusivity drops off faster than the porosity until the curves intersect. Then the porosity curve lies above the diffusivity curve. The two curves will then intersect again when the porosity falls to zero. This type of behavior can be accounted for only if the combination of bulk and Knudsen diffusivity is considered.

In Figure 6 plots of conversion and reaction rate as a function of dimensionless radius near the end of the reaction are shown. It can be seen that the more open pore structure of the calcined limestone used for experiment E-0-19 (dashed line) allows for deep penetration into the pellet, whereas for experiment E-0-14 (solid line) we see a much sharper break in the level of the local conversion at a dimensionless radius of 0.7. The difference in pore structures manifests itself even more dramatically in the reaction rate curves. Experiment E-0-19 displays a broad peak because of the broad distribution of conversion due to the broader initial pore size distribution. Experiment E-0-14 however displays a much sharper peak because most of the pores are small. The smaller pores react more quickly than larger pores and set up a greater resistence to diffusion in the pellet. The peaks in reaction rate occur because of the combined effects of the gas concentration profile and the local conversion profile. These plots dramatically display the differences in behavior obtained from different pore-size distributions.

In Figure 7 the pore size distribution at various values of the cumulative gas concentration (τ) is presented. In this plot we see how the distribution evolves with extent of reaction, which gives insight into the observed changes of the macroscopic properties of the pellet. At very low levels of conversion (τ = 2.5 s), most of the changes in the pore size and volume occur in the small pores ($<10^{-7}$ m). This is expected because of the much larger surface to volume ratio in the small pores. At low levels of conversion these

small, high surface area pores are eliminated, resulting in a steep initial drop in the local reactivity (K_e) of the porous medium. At larger levels of conversion ($\tau = 250$ s) most of the porosity is associated with the larger ($>10^{-7}$ m) pores which begin to experience significant changes in pore size and volume. It is these large pores near the outside of the pellet which control the rate of diffusion into the reacting pellet at the higher levels of conversion. The result is a gradual decrease in the reaction rate as observed in the experiments. This plot illustrates the difficulty of modeling the behavior of an evolving distribution with a single average pore or grain size.

NOTATION

c = gas reactant concentration in porous matrix
$\hat{c}$ = gas reactant concentration in solid product layer
c_o = bulk gas reactant concentration outside reacting pellet
D = dimensionless effective diffusivity (D_e/D_o)
D_c = combined bulk and Knudsen diffusivity of reactant gas in a particular pore
D_B = bulk diffusivity of reactant gas
D_e = effective diffusivity of reactant gas through porous matrix
D_k = Knudsen diffusivity of reactant gas
D_o = initial diffusivity of reactant gas through porous matrix before any reaction occurs
D_s = effective diffusivity of reactant gas through solid product layer
K = dimensionless effective reactivity (K_e/K_o)
K_e = effective reactivity of porous matrix
K_o = initial reactivity of porous matrix before any reaction occurs
k = surface reaction rate constant
k_g = mass transfer coefficient surrounding reacting pellet
l = length of a pore
P = porosity
R = radial position in spherical pellet
R_o = radius of spherical pellet
r = radial position of a cylindrical pore
r_o = initial radius of a cylindrical pore before reaction
r_1 = radial position of gas/solid interface in a cylindrical pore
r_2 = radial position of solid product/solid reactant interface in a cylindrical pore
Sh = Sherwood Number ($2k_gR_o/D_B$)
t = time
V_A, V_B = molar volumes of solid reactant A and solid product B
x = local conversion of solid reactant A at a particular location in pellet
α = ratio of molar volumes of the solid product B to solid reactant A
β_i = stoichiometric coefficient of component i
ϵ = void volume per unit volume (porosity)
ϵ_o = initial porosity of porous matrix
ζ = tortuosity
η_1 = number of pores intersecting a unit area per unit radius (r_1) of cylindrical pore
η_2 = number of pores intersecting a unit area per unit radius (r_2) of cylindrical pore
λ = dimensionless constant defined in Eq. 9
ξ_1 = rate of change of r_1 with respect to τ
τ = conversion parameter defined in Eq. 6
ϕ = net fraction of pores gained due to pore intersections
ψ = void area per unit area

ACKNOWLEDGMENT

The authors gratefully acknowledge the financial support of the Texas Energy and Natural Resources Advisory Council and the U.S. Department of Energy. Also we would like to thank Westinghouse for supplying the experimental data used in this paper.

LITERATURE CITED

Bhatia, S. K., and D. D. Perlmutter, "A Random Pore Model for Fluid-Solid Reactions: I. Isothermal, Kinetic Control," *AIChE J.*, **26**, No. 3, 379 (1980).

Bhatia, S. K., and D. D. Perlmutter, "A Random Pore Model for Fluid-Solid Reactions: II. Diffusion and Transport Effects," *AIChE J.*, **27**, No. 2, 247 (1981a).

Bhatia, S. K., and D. D. Perlmutter, "The Effect of Pore Structure on Fluid-Solid Reactions: Applications to SO_2-Lime Reaction," *AIChE J.*, **27**, No. 2, 226 (1981b).

Borgwardt, R. H., "Kinetics of the Reaction of SO_2 with Calcined Limestone," *Envr. Sci. Tech.*, **4**, 59 (1970).

Calvelo, A., and J. M. Smith, "Intrapellet Transport in Gas-Solid Non-Catalytic Reactions," *Proceedings of Chemeca 70*, Paper 3.1, Butterworths Australia (1971).

Christman, P. G., "Analysis of Simultaneous Diffusion and Chemical Reaction in the Calcium Oxide/Sulfur Dioxide System," Ph.D. Dissertation, The University of Texas, Austin (1981).

Chrostwoski, J. W., and C. Georgakis, "Pore Plugging Model for Gas-Solid Reactions," *ACS Symp. Ser.*, No. 65, *Chemical Reaction Engineering*, Houston (1978).

Chu, C., "Parallel Plate Model for Non-Catalytic Gas-Solid Reactions," *Chem. Eng. Sci.*, **27**, 367 (1974).

Dudukovic', M. P., "Note on Gas Solid Non-catalytic Reactions," *AIChE J.*, **22**, No. 5 (1976).

Fuller, E. N., P. D. Schettler, and J. C. Giddings, "New Method for Prediction of Binary Gas-Phase Diffusion Coefficients," *Ind. Eng. Chem.*, **58**, No. 5, 18 (1966).

Georgakis, C., C. W. Chang, and J. Szekely, "A Changing Grain Size Model for Gas Solid Reactions," *Chem. Eng. Sci.*, **34**, 1072 (1979).

Hartman, M., and R. W. Coughlin, "Reaction of Sulfur Dioxide with Limestone and The Grain Model," *AIChE J.*, **22**, No. 3, 490 (1976).

Hashimoto, K. K., and P. L. Silveston, "Gasification: Part I. Isothermal Kinetic Control Model for a Solid with a Pore Size Distribution," *AIChE J.*, **19**, No. 2, 259 (1973a).

Hashimoto, K. K., and P. L. Silveston, "Gasification: Part II. Extension to Diffusion Control," *AIChE J.*, **19**, No. 2, 268 (1973b).

Johnson, M. F. L., and W. E. Stewart, "Pore Structure and Gaseous Diffusion in Solid Catalysis," *J. Cat.*, **4**, 248 (1965).

Lieberman, R. W., "Equilibrium and Thermodynamic Properties of Complex Chemical Mixtures," Westinghouse Research and Development Center, Pittsburgh, PA (1970).

Petersen, E. E., "Reactions in Porous Solids," *AIChE J.*, **3**, No. 4, 443 (1957).

Ramachandran, P. A., and J. M. Smith, "A Single-Pore Model for Gas-Solid Non-Catalytic Reactions," *AIChE J.*, **23**, No. 3, 353 (1977a).

Ramachandran, P. A., and J. M. Smith, "Effect of Sintering and Porosity Changes on Rates of Gas-Solid Reactions," *Chem. Eng. J.*, **14**, 137 (1977b).

Ranade, P. V., and D. P. Harrison, "The Grain Model Applied to Porous Solids with Varying Structural Properties," *Chem. Eng. Sci.*, **34**, 427 (1979).

Schechter, R. S., and J. L. Gidley, "The Change in Pore Size Distribution from Surface Reactions in Porous Media," *AIChE J.*, **15**, No. 3, 339 (1969).

Simons, G. A., and M. L. Finson, "The Structure of Coal Char: Part I. Pore Branching," *Combustion Sci. and Tech.*, **19**, 217 (1979).

Simons, G. A., "The Structure of Coal Char: Part II. Pore Combination," *Combustion Sci. and Tech.*, **19**, 227 (1979).

Szekely, J., and J. W. Evans, "A Structural Model for Gas-Solid Reactions with a Moving Boundary," *Chem. Eng. Sci.*, **25**, 1091 (1970).

Szekely, J., and J. W. Evans, "A Structural Model for Gas-Solid Reactions with a Moving Boundary—II. The Effect of Grain Size, Porosity and Temperature on the Reaction of Porous Pellets," *Chem. Eng. Sci.*, **26**, 1901 (1971).

Szekely, J., J. W. Evans, and H. Y. Sohn, *Gas-Solid Reactions*, Chapter 3, Academic Press, Inc., New York (1976).

Ulerich, N. H., E. P. O'Neill, and D. L. Keairns, "The Influence of Limestone Calcination on the Utilization of the Sulfur Solvent in Atmospheric Pressure Fluid-Bed Combustors," EPRI FP-426, Final Report (1977).

Weast, R. C., *Handbook of Chemistry and Physics*, Section B, 52nd ed., Chemical Rubber Co., Cleveland, OH (1971).

Wen, C. Y., and M. Ishida, "Reaction Rate of Sulfur Dioxide with Particles Containing Calcium Oxide," *Env. Sci. and Tech.*, **7**, 703 (1973).

Manuscript received June 22, 1981; revision received June 16, and accepted June 29, 1982.